Supplementary information for

Diatom Frustules as a Biomineralised Scaffold for the Growth of Molybdenum Disulfide Nanosheets

Edward A. Lewis,[a] David J. Lewis,[a,b,]* Aleksander A. Tedstone,[b] Georgia Kime,[c] Simon Hammersley,[c] Philip Dawson,[c] David J. Binks,[c] Paul O'Brien[a,b]* and Sarah J. Haigh[a*]

[a] School of Materials, University of Manchester, M13 9PL, UK.

[b] School of Chemistry, University of Manchester, M13 9PL, UK.

[c] Photon Science Institute, University of Manchester, M13 9PL, UK.

*David.lewis-4@manchester.ac.uk, Paul.o'brien@manchester.ac.uk, Sarah.haigh@manchester.ac.uk

Experimental

Synthesis of DE-MoL$_4$

The synthesis and characterisation of Tetrakis(diethyldithiocarbamato)molybdenum(IV), **MoL$_4$**, is described previously.[1-2] **MoL$_4$** was synthesised by oxidative addition of tetraethyldithiuram to molybdenum(0) hexacarbonyl. Briefly, 3.7 mmol of molybdenum hexacarbonyl (1.0 equiv) was heated to reflux in acetone (40 mL) in the presence of 7.4 mmol of tetraethylthiuram (2.0 equiv), the mixture was held at this temperature for 2 hours and then allowed to cool slowly to room temperature over an hour. A black crystalline solid formed, which was isolated by filtration and washed with pentane (3 × 20 mL). All characterisation agreed with that reported previously by Lewis et al.[1]

50mg of **MoL$_4$** was dissolved in 5 ml of tetrahydrofuran and 300 mg of Celite[TM] was added to the resulting solution. The suspension was then stirred for 30 minutes in an open beaker at room temperature before the solid product, **DE-MoL$_4$**, was removed by filtration. **DE-MoL$_4$** is an orange powder, in contrast to the white Celite[TM] indicating successful impregnation with the molybdenum precursor, however, the filtrate was observed to have a dark red colour, suggesting that a significant amount of **MoL$_4$** remained in the solution.

Synthesis of DE-MoS$_2$

After drying in air the **DE-MoL$_4$** was transferred to an Alumina crucible and loaded into quartz tube with one closed end. The open end of the quartz tube was connected to a Schlenk line and standard Schlenk line techniques were used to ensure that the sample was under a N$_2$ atmosphere. The tube was then inserted into a Carbolite tube furnace, preheated to a temperature of 450°C, the furnace was held at this temperature for 30 minutes after which time the tube was removed and allowed to cool to room temperature. A black powder, **DE-MoS$_2$**, was removed from the crucible.

Characterisation

Raman spectroscopy was performed using a Renishaw 1000 microscope system equipped with a 100 x objective, with solid-state laser excitation (514.5 nm, 1% power). The incident light was linearly polarized in the sample plane with scattered light left unanalyzed for collection by the air cooled CCD. Bright-field images were collected using a standard CCD camera.

~6 mg of **DE-MoL$_4$** was analysed by thermogravimetric analysis (TGA). TGA was performed by the University of Manchester Microanalytical Laboratory, using a Thermo Scientific Flash 2000 Organic Elemental Analyzer and a Seiko SSC/S200 model using a heating rate of 10 °C min^{-1} from room temperature to 600 °C in a nitrogen atmosphere.

SEM samples were prepared by mounting a carbon double-sided adhesive disc on an aluminium pin stub and dusting the carbon disc with **DE-MoS$_2$**. SEM imaging and analysis was performed using a Zeiss Sigma VP field emission gun scanning electron microscope (FEG-SEM) equipped with an Oxford Instruments X-maxN 150 silicon drift detector (SDD). For secondary electron (SE) and backscatted electon (BSE) imaging the instrument was operated at 2 kV. While for energy dispersive x-ray (EDX) analysis an accelerating voltage of 30 kV was used, EDX spectrum images were acquired using the AZTEC analysis system, the software's TruMap function was used to deconvolute the overlapping Mo L$_\alpha$ and S K$_\alpha$ peaks.

To prepare samples for STEM analysis, **DE-MoL$_4$** was sonicated in chloroform to detach some of the surface flakes the resulting solution was drop cast onto a holey carbon Cu TEM grid. STEM imaging and EDX analysis was performed in a probe-side aberration corrected FEI Titan G2 80-200 ChemiSTEM microscope equipped with a Super-X EDX detector system and operated at 200 kV. For HAADF imaging a probe current of ~90 pA, convergence angle of 26 mrad and a detector inner angle of 48 mrad were used. EDX spectrum images were acquired with the sample at 0° tilt and with all four of the microscope's silicon drift detectors turned on. STEM images were recorded in FEI TIA software and EDX data was recorded and analysed using Bruker Esprit, the software's QMap function was used to deconvolute the overlapping Mo L$_\alpha$ and S K$_\alpha$ peaks.

Reflectance spectra were acquired for samples of **DE** and **DE-MoS$_2$** using a Perkin Elmer Lambda 1050 UV/Vis/IR spectrophotometer with an integrating sphere. Low temperature photoluminescence (PL) spectroscopy was performed on **DE** and **DE-MoS2** samples mounted on indium foil and cooled in a closed-cycle helium cryostat down to a temperature of 11.4 K. Excitation was provided by a continuous wave HeCd laser (Kimmon, IK3101R-D) emitting at a wavelength of 325 nm. The excitation beam had a power of 1 mW and was focussed by a +15 cm focal length lens to a spot on the sample with a FWHM diameter of 30 μm. The PL thus produced was collected and focussed into a spectrophotometer incorporating a CCD array (Jobin Yovin iHR550) after passing through a long-pass filter with a cut-on wavelength of 475 nm to remove scattered laser light.

Grazing incidence X-ray diffraction (XRD) patterns were acquired using a Bruker D8 Advance diffractometer, using a Cu Kα source with a Göbel mirror optic and Soller slits on the detector side. Scans were acquired at a grazing incidence of 3° over a 2θ range of 5–80° with 0.02° steps.
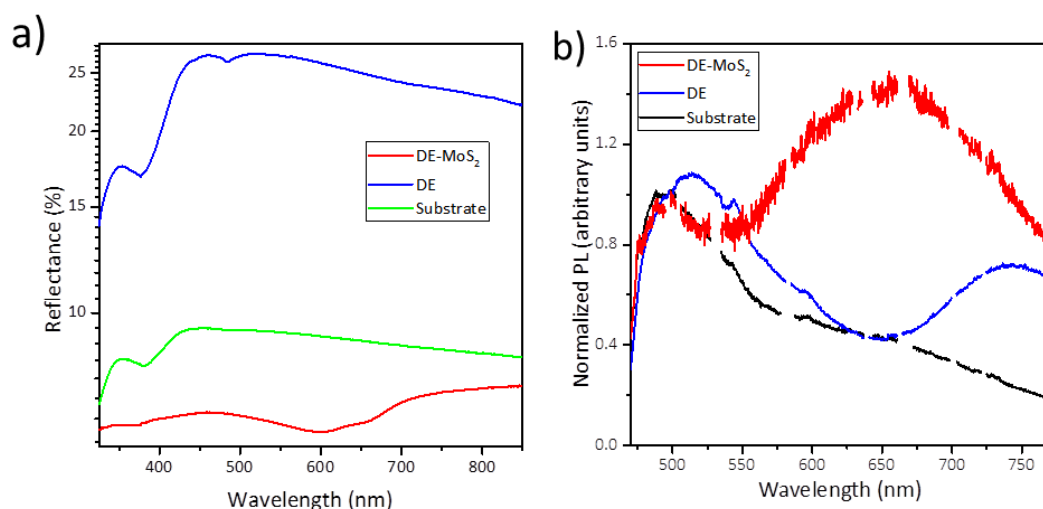
Precursor decomposition

Heating the precursor **MoL$_4$** to 450$^°$C results in its decomposition to form MoS$_2$, this reaction has previously been used in the aerosol assisted chemical vapour deposition (AACVD) synthesis of MoS$_2$ thin films and Cr doped MoS$_2$ films.[1, 3] Dithiocarbamate complexes and related precursor have been widely used in the synthesis of metal chalcogenide nanocrystals and thin films, they typically decompose cleanly at relatively low temperature to give pure metal sulphide products.[4-7] The mechanism of decomposition for the related Xanthate family of precursors is widely agreed to occur via the Chugaev elimination reaction,[8-10] while the mechanism of dithiocarbamate decomposition is less well studied, work on the decomposition of diselenocarbamato complexes suggests that an analogous β elimination involving a cyclic intermediate may occur, however, it is also noted that changes to the substituents at the nitrogen can have a significant effect on the precursor's decomposition.[11] Thermogravimetric analysis of **MoL$_4$** shows that complete conversion to MoS$_2$ should occur above 400$^°$C. Previous studies which have used this precursor in AACVD have used reaction temperatures ranging from 400-500$^°$C,[1, 3] while MoS$_2$ can be formed at any temperature within this range these reports suggest that the reaction temperature may affect product morphology. Specifically, Adeogun et al. report that MoS$_2$ films formed at ≥ 450$^°$C are composed of platelets while lower temperature (400 and 425$^°$C leads to the formation of MoS$_2$ rods and tubes.[3]

Photoluminescence and UV-visible spectroscopy

Reflectance spectra were acquired for samples of DE and DE-MoS$_2$ and are shown in SI Fig. 1a. For these measurements, 15 mg of the powdered samples were fixed to a glass substrate using 150 mg of epoxy resin; the reflectance spectrum for a reference epoxy resin-coated glass substrate is also given in SI Fig. 1a for comparison. The reflectance for the DE-MoS$_2$ sample is less than that of the DE sample across the spectrum, and increasingly so for shorter wavelengths, which is consistent with the absorption spectrum of atomically-thin MoS$_2$.[12-13] Furthermore, local reflection minima are also evident at ~660 nm and 610 nm, which can be attributed to the absorption peaks associated with the A and B excitons of atomically-thin MoS$_2$, which form due to valence band splitting at the direct-gap K point in atomically thin MoS$_2$.[12-13]

SI Fig. 1b shows the low temperature PL spectra obtained for the DE-MoS$_2$ and DE samples, and the indium substrate; the spectra have been corrected for the system response and scaled to be of equal intensity at 500 nm, the peak of the substrate emission, for ease of comparison. Emission from the DE only sample is similar to that previously reported and arises from surface defects and oxygen hole centres.[14] Some PL is also seen from the substrate, particularly at short wavelengths. However for the DE-MoS$_2$ sample, in addition to the contributions from the DE and indium, broad emission can also be seen between 550 – 750 nm. This is attributed to emission from the MoS$_2$ due to the recombination of A and B excitons, and of negatively-charged trions. The A and B excitons are commonly reported to produce emission between 600-700 nm.[12-13] Trion recombination can also contribute to the PL , a state which forms when a trapped electron from a dissociated exciton is captured by a second A exciton, and exhibits emission energies around 18meV lower than the A exciton emission.[15] Each of these emission energies depends on sample thickness,[16] so an ensemble sample such as this will exhibit broadening, leading to the wide emission feature seen.
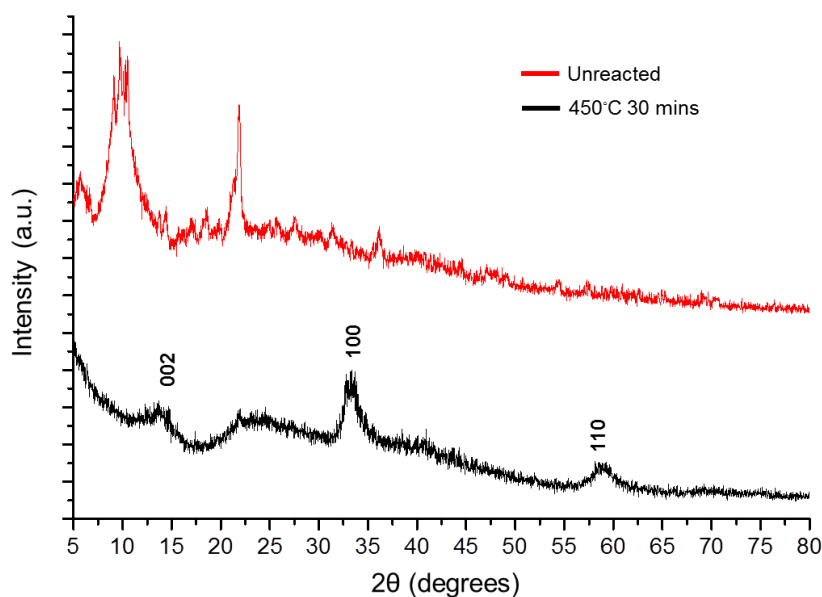
SI Fig. 1 (a) Reflectance and (b) low temperature photoluminescence spectra for the DE-MoS$_2$ and DE samples. The spectra obtained for the substrates only are also shown for comparison. Note that the gaps in the PL spectra are due to the removal of plasma lines emitted by the laser.

Surface area analysis

BET surface areas were determined for both **DE** and **DE-MoS$_2$**, giving values of 0.74 and 0.68 m^2/g respectively. These values are lower than but on the same order of magnitude as previous reports of diatom frustules having a surface area of 1.65 m^2/g.[17] Given the rich variety of diatom morphologies and the inhomogeneity of diatomous earth such variation does not seem unfeasible if the samples are from different source of have been treated differently. The fact that the surface area decreases slightly upon MoS$_2$ decoration seems consistent with the observation the MoS$_2$ fills pores in the frustule's surface. For potential catalytic application, where considerably higher surface areas would be desirable the formation of silicon replicas of the silica frustules, prior to MoS$_2$ decoration, could be a promising approach, a dramatic increase in surface area (from 1.65 to 541 m^2/g) has been reported to accompany this transformation due to the formation of a large number of ≤2 nm pores in the replicas.[17]

X-ray diffraction

In addition to the evidence provided by Raman spectroscopy and atomic resolution STEM imaging, further proof of the formation of MoS$_2$ is provided by X-ray diffraction (XRD). XRD patterns of thin films of the unreacted precursor show a number of characteristic peaks, especially a strong peak at 2θ ≈ 10°C. After heating at 450°C for 30 minutes, these characteristic peaks have disappeared and are replaced by three peaks which can be indexed to the {002}, {100} and {110} planes of MoS$_2$. This result is consistent with our belief that the heat treatment used in this work brings about complete conversion of the precursor to crystalline MoS$_2$. The broad peaks seen in the pattern are to be expected given the small crystallite dimensions observed by electron microscopy. It is noted that the XRD pattern seen here shows a close resemblance to those reported in other studies of MoS$_2$ nanomaterials.[18-20] The ~1% MoS$_2$ loading of the **DE-MoS$_2$** samples meant that detection of clear MoS$_2$ peaks from these samples was beyond the sensitivity of our experiments.

SI Fig. 2. Grazing incidence XRD of thin films of unreacted **MoL₄** before and after heating at 450 °C for 30 minutes. The post annealing sample shows broad peaks indexed to the {002}, {100}, and {110} planes of MoS₂.
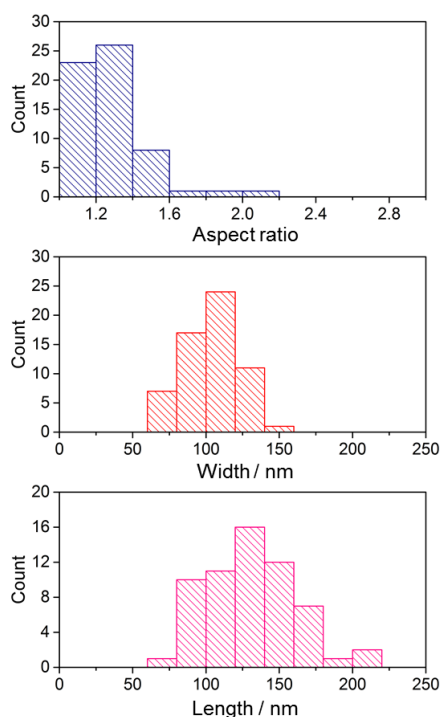
Thermogravimetric analysis

The clean decomposition of **MoL₄** to give MoS_2 has previously been demonstrated by thermogravimetric analysis (TGA).[21] An identical shaped curve to that seen for decomposition of pure **MoL₄** is observed when **DE-MoL₄** is heated; suggesting that 100% conversion of **MoL₄** to MoS_2 is achieve at reaction temperatures above 400°C. Complete conversion to MoS_2 is supported by other characterisation techniques which show no evidence of oxides or unreacted precursor in **DE-MoS₂**. While the curve shapes are the same for TGA of **MoL₄** and **DE-MoL₄**, the mass loss observed for **DE-MoL₄** is dramatically less, due to the majority of the specimen mass being inert silica. This mass loss can be used to estimate the MoS_2 loading: the 3.5 % mass loss seen in the TGA curve should correspond to **DE-MoS₂** being ~1.1% MoS_2 by mass. This value is consistent with the Mo content determined by inductively coupled atomic emission spectroscopy.
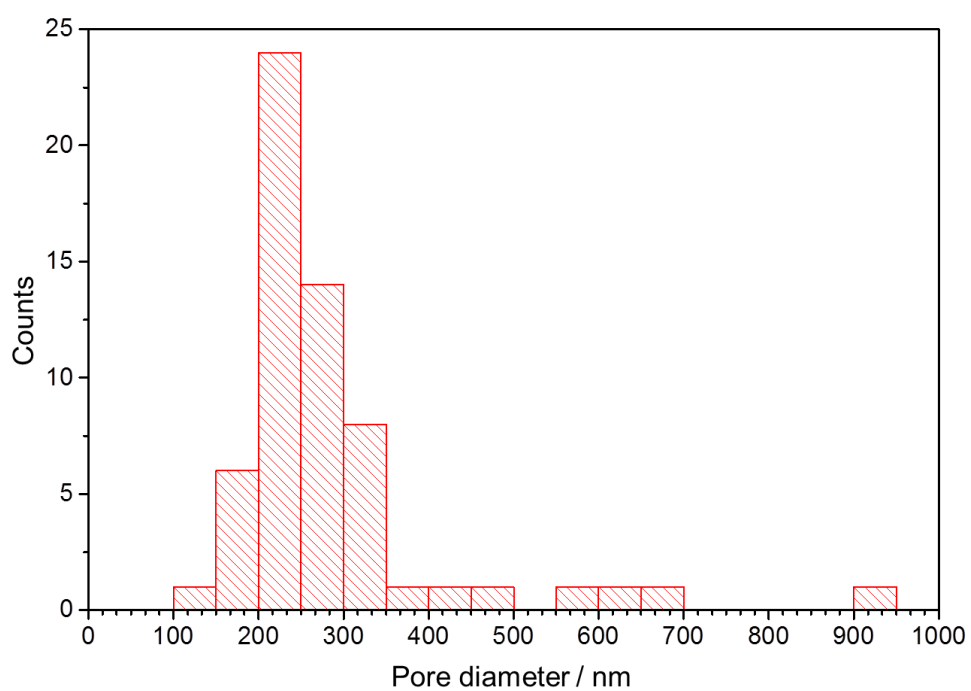
Raman spectroscopy

Raman spectroscopy is a widely used tool for assessing the thickeness of two dimensional materials.[22] The Raman spectra of MoS_2 have been shown to exhibit thickness dependent features.[23-24] While peak widths and intensities are influenced by thickness,[24] it is the Raman frequencies of the E^1_{2g} and A_{1g} modes that are generally considered to allow accurate determination of the number of layers.[23-24] The Raman spectra for **DE-MoS₂** shown in Fig. 1 of this manuscript shows two strong peaks centred at 382 and 408 cm^{-1} which are assigned to the E_{2g} and A_{1g} modes of MoS_2. These spectra strongly supported the formation of crystalline MoS_2 and the absence of either unreacted precursor or oxidised by-products. Frequencies of ~385 cm^{-1} and ~403 cm^{-1} have been reported for

monolayer material, with the E^1_{2g} and A_{1g} separation increasing as layer thickness increases, and frequencies of ~383 cm^{-1} and ~408 cm^{-1} correspond to bulk MoS$_2$.[24] The E$_{2g}$ and A$_{1g}$ frequencies observed in spectra of **DE-MoS$_2$** are, therefore, consistent with bulk MoS$_2$. It should, however, be noted, that Raman's thickness sensitivity only allows identification of thickness ≤4 layers, with sheets >4 layers thick giving approximately bulk-like Raman frequencies.[24] Furthermore the literature on Raman spectroscopy of MoS$_2$ is based upon mechanically exfoliated sheets.[23-24] The spectra reported in such studies are taken from a single crystalline sheet, typically several µm in diameter, on flat SiO$_2$ substrates,[23-24] in contrast the spectra reported in this study will be an ensemble average of thousands of small flakes with lateral dimensions rarely exceeding 10 nm. Furthermore, the flakes are randomly oriented and supported on a highly curved and porous substrate (the diatom frustule). It is unclear how readily data from single large flakes can be applied to ensembles of small flakes and whether factors such small lateral flake dimensions will significantly affect the frequency of Raman modes. However, assuming such factors are not significant we conclude that the average thickness of the MoS$_2$ flake population in **DE-MoS$_2$** is > 4 layers, this is not necessarily inconsistent with HAADF STEM observations suggesting a range of flake thicknesses from monolayer to 6-layers thick.
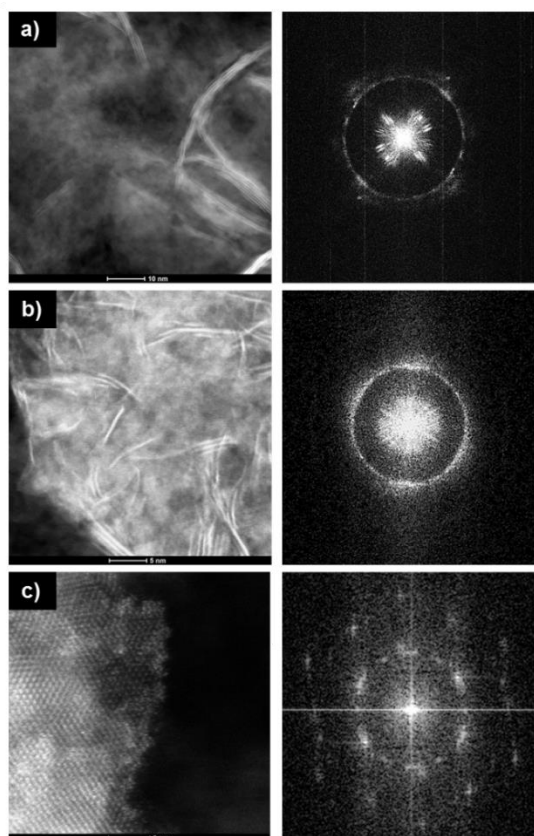
SEM size analysis

SI Fig. 3. Size analysis of flakes observed on frustule surface in SE SEM images, histograms based on measurement of 60 flakes.
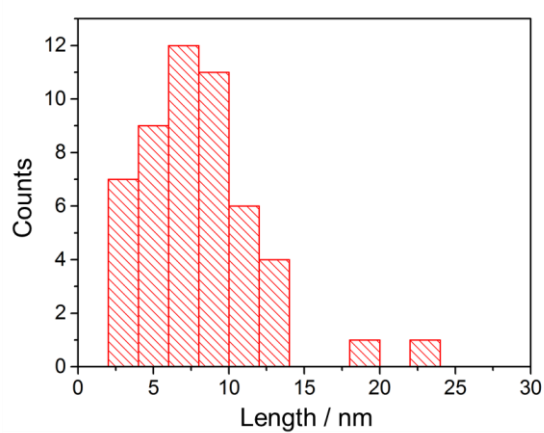
SI Fig. 4. Size analysis of pores observed on frustule surfaces in SE SEM images, histogram based on measurement of 60 pores. The mean pore size is found to be 281 nm. The size of underlying pores is not believed to change upon heating due to the melting point of silica being considerably higher than the reaction temperature. However, there is some infilling of the pores with MoS_2 flakes as evidenced in SEM images and by the reduced surface area seen in BET measurements.
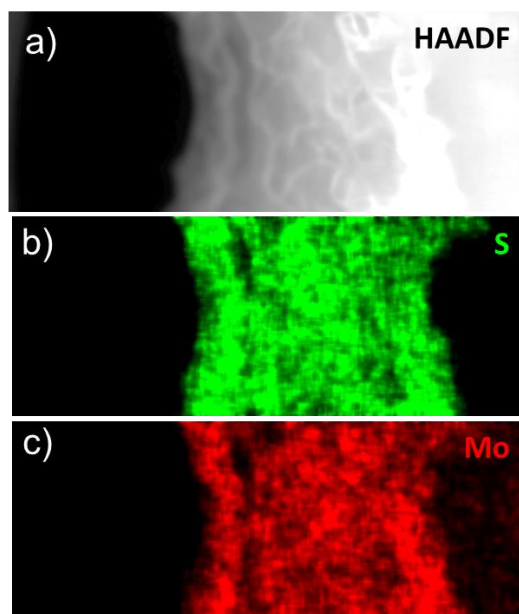
Further STEM analysis

SI Fig. 5. Atomic resolution HAADF STEM images of MoS$_2$ structures extracted from **DE-MoS$_2$**, (a) and (b) show regions comprised of numerous flakes oriented both side on and with their basal planes parallel to the support. The corresponding fourier transforms (FTs) show ring patterns corresponding to the MoS$_2$ {100} planes, demonstrating the polycrystalline nature of these structures resulting from the aggregation of multiple small sheets. (c) shows a region of single crystalline MoS$_2$, many single crystal regions can be found but their lateral dimensions rarely exceed 10 nm.
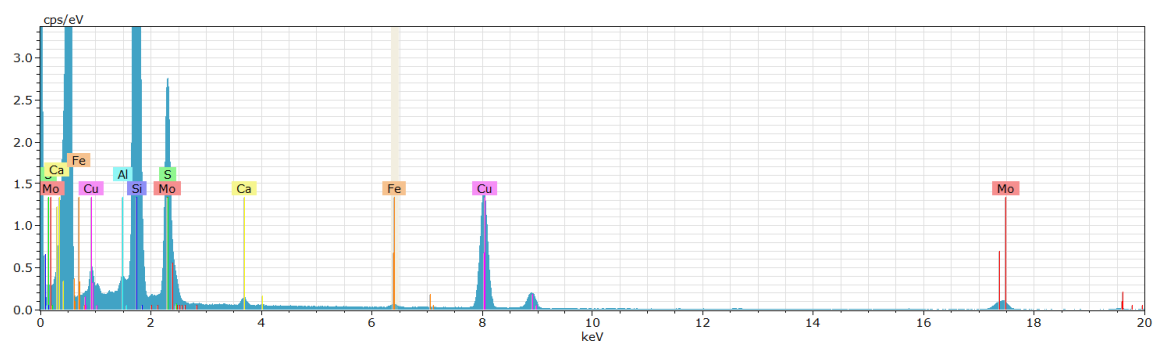

SI Fig. 6. Sheet lateral dimensions based on measurement of 50 side-on sheets found in HAADF STEM images.

Further EDX analysis

SI Fig. 7. Deconvoluted EDX maps corresponding to Fig. 4. Due to the overlap of Mo L_α and S K_α peaks it is necessary to deconvolute the spectrum image to ensure that Mo and S counts are truly colocalised, Bruker Esprit software's QMap function was used to do this, the resulting S and Mo maps (b and c) strongly support colocalisation.

SI Fig. 8. Summed EDX spectrum extracted from the STEM EDX spectrum image shown in Fig. 4 and SI Fig. 7.

References

1.   Lewis, D. J.; Tedstone, A. A.; Zhong, X. L.; Lewis, E. A.; Rooney, A.; Savjani, N.; Brent, J. R.; Haigh, S. J.; Burke, M. G.; Muryn, C. A.; Raftery, J. M.; Warrens, C.; West, K.; Gaemers, S.; O'Brien, P., Thin Films of Molybdenum Disulfide Doped with Chromium by Aerosol-Assisted Chemical Vapor Deposition (AACVD). *Chem Mater* **2015,** *27* (4), 1367-1374.

2.   Decoster, M.; Conan, F.; Guerchais, J. E.; Le Mest, Y.; Sala Pala, J.; Jeffery, J. C.; Faulques, E.; Leblanc, A.; Molinie, P., Radical cation-radical anion salts: Molybdenum complexes containing the [TCNQ]•− or [TCNE]•− radical anions. X-ray crystal structure of [Mo(Et2NCS2)4](TCNQ). *Polyhedron* **1995,** *14* (13), 1741-1750.

3.   Adeogun, A.; Afzaal, M.; O'Brien, P., Studies of Molybdenum Disulfide Nanostructures Prepared by AACVD Using Single-Source Precursors. *Chem Vap Deposition* **2006,** *12* (10), 597-599.

4.   Malik, M. A.; Afzaal, M.; O'Brien, P., Precursor Chemistry for Main Group Elements in Semiconducting Materials. *Chemical Reviews* **2010,** *110* (7), 4417-4446.

5.   Fan, D.; Afzaal, M.; Mallik, M. A.; Nguyen, C. Q.; O'Brien, P.; Thomas, P. J., Using coordination chemistry to develop new routes to semiconductor and other materials. *Coordination Chemistry Reviews* **2007,** *251* (13-14), 1878-1888.

6.   Pickett, N. L.; O'Brien, P., Syntheses of semiconductor nanoparticles using single-molecular precursors. *Chem Rec* **2001,** *1* (6), 467-479.

7.   Lewis, E.; Haigh, S.; O'Brien, P., The synthesis of metallic and semiconducting nanoparticles from reactive melts of precursors. *J. Mater. Chem. A* **2014,** *2* (3), 570-580.

8.   Pradhan, N.; Katz, B.; Efrima, S., Synthesis of high-quality metal sulfide nanoparticles from alkyl xanthate single precursors in alkylamine solvents. *Journal of Physical Chemistry B* **2003,** *107* (50), 13843-13854.

9.   Alam, N.; Hill, M. S.; Kociok-Köhn, G.; Zeller, M.; Mazhar, M.; Molloy, K. C., Pyridine Adducts of Nickel(II) Xanthates as Single-Source Precursors for the Aerosol-Assisted Chemical Vapor Deposition of Nickel Sulfide. *Chemistry of Materials* **2008,** *20* (19), 6157-6162.

10.   Clark, J. M.; Kociok-Kohn, G.; Harnett, N. J.; Hill, M. S.; Hill, R.; Molloy, K. C.; Saponia, H.; Stanton, D.; Sudlow, A., Formation of PbS materials from lead xanthate precursors. *Dalton Transactions* **2011,** *40* (26), 6893-6900.

11.   Chunggaze, M.; Azad Malik, M.; O'Brien, P., Studies of the thermal decomposition of some diselenocarbamato complexes of cadmium or zinc: molecular design for the deposition of MSe films by CVD. *Journal of Materials Chemistry* **1999,** *9* (10), 2433-2437.

12.   Mak, K. F.; Lee, C.; Hone, J.; Shan, J.; Heinz, T. F., Atomically thin MoS 2: a new direct-gap semiconductor. *Physical Review Letters* **2010,** *105* (13), 136805.

13.   Wang, Q. H.; Kalantar-Zadeh, K.; Kis, A.; Coleman, J. N.; Strano, M. S., Electronics and optoelectronics of two-dimensional transition metal dichalcogenides. *Nat Nano* **2012,** *7* (11), 699-712.

14.   Jeffryes, C.; Solanki, R.; Rangineni, Y.; Wang, W.; Chang, C. h.; Rorrer, G. L., Electroluminescence and photoluminescence from nanostructured diatom frustules containing metabolically inserted germanium. *Advanced Materials* **2008,** *20* (13), 2633-2637.

15.   Mak, K. F.; He, K.; Lee, C.; Lee, G. H.; Hone, J.; Heinz, T. F.; Shan, J., Tightly bound trions in monolayer MoS2. *Nature materials* **2013,** *12* (3), 207-211.

16.   Eda, G.; Yamaguchi, H.; Voiry, D.; Fujita, T.; Chen, M.; Chhowalla, M., Photoluminescence from chemically exfoliated MoS2. *Nano letters* **2011,** *11* (12), 5111-5116.

17.   Bao, Z.; Weatherspoon, M. R.; Shian, S.; Cai, Y.; Graham, P. D.; Allan, S. M.; Ahmad, G.; Dickerson, M. B.; Church, B. C.; Kang, Z.; Abernathy Iii, H. W.; Summers, C. J.; Liu, M.; Sandhage, K. H., Chemical reduction of three-dimensional silica micro-assemblies into microporous silicon replicas. *Nature* **2007,** *446* (7132), 172-175.

18.   Sun, P.; Zhang, W.; Hu, X.; Yuan, L.; Huang, Y., Synthesis of hierarchical MoS2 and its electrochemical performance as an anode material for lithium-ion batteries. *Journal of Materials Chemistry A* **2014,** *2* (10), 3498-3504.

19.   Zhang, R.; Li, Y.; Qi, J.; Gao, D., Ferromagnetism in ultrathin MoS2 nanosheets: from amorphous to crystalline. *Nanoscale research letters* **2014,** *9* (1), 1-5.

20.   Vattikuti, S. P.; Byon, C., Synthesis and Characterization of Molybdenum Disulfide Nanoflowers and Nanosheets: Nanotribology. *Journal of Nanomaterials* **2015,** *2015*.

21.   McCain, M. N.; He, B.; Sanati, J.; Wang, Q. J.; Marks, T. J., Aerosol-Assisted Chemical Vapor Deposition of Lubricating MoS2 Films. Ferrous Substrates and Titanium Film Doping. *Chemistry of Materials* **2008,** *20* (16), 5438-5443.

22.   Ferrari, A. C.; Meyer, J. C.; Scardaci, V.; Casiraghi, C.; Lazzeri, M.; Mauri, F.; Piscanec, S.; Jiang, D.; Novoselov, K. S.; Roth, S.; Geim, A. K., Raman Spectrum of Graphene and Graphene Layers. *Physical Review Letters* **2006,** *97* (18), 187401.

23.   Lee, C.; Yan, H.; Brus, L. E.; Heinz, T. F.; Hone, J.; Ryu, S., Anomalous lattice vibrations of single-and few-layer MoS2. *ACS nano* **2010,** *4* (5), 2695-2700.

24.   Li, H.; Zhang, Q.; Yap, C. C. R.; Tay, B. K.; Edwin, T. H. T.; Olivier, A.; Baillargeat, D., From Bulk to Monolayer MoS2: Evolution of Raman Scattering. *Advanced Functional Materials* **2012,** *22* (7), 1385-1390.